Published in final edited form as:
Neuron. 2010 August 12; 67(3): 466–479. doi:10.1016/j.neuron.2010.06.034.

Selective Activation of Striatal Fast Spiking Interneurons during Choice Execution

Gregory J. Gage[1], **Colin R. Stoetzner**[2], **Alexander B. Wiltschko**[3], and **Joshua D. Berke**[2,3]

[1] Department of Biomedical Engineering, University of Michigan, Ann Arbor, MI, 48109

[2] Neuroscience Program, University of Michigan, Ann Arbor, MI, 48109

[3] Department of Psychology, University of Michigan, Ann Arbor, MI, 48109

Abstract

Basal ganglia circuits are essential for the organization and execution of voluntary actions. Within the striatum, fast-spiking interneurons (FSIs) are thought to tightly regulate the activity of medium-spiny projection neurons (MSNs) through feed-forward inhibition, yet few studies have investigated the functional contributions of FSIs in behaving animals. We recorded presumed MSNs and FSIs together with motor cortex and globus pallidus (GP) neurons, in rats performing a simple choice task. MSN activity was widely distributed across the task sequence, especially near reward receipt. By contrast, FSIs showed a coordinated pulse of increased activity as chosen actions were initiated, in conjunction with a sharp decrease in GP activity. Both MSNs and FSIs were direction-selective, but neighboring MSNs and FSIs showed opposite selectivity. Our findings suggest that individual FSIs participate in local striatal information processing, but more global disinhibition of FSIs by GP is important for initiating chosen actions while suppressing unwanted alternatives.

INTRODUCTION

Dysfunction of the basal ganglia (BG) can produce a range of neurological and psychiatric symptoms, including slowness or paucity of movement in Parkinson's Disease and uncontrolled or unwanted actions and thoughts in Huntington's Disease, Tourette Syndrome and obsessive-compulsive disorder. In normal individuals there is evidence for BG involvement in multiple stages of the control of voluntary action, including motivation towards goals (Balleine & O'Doherty 2010), selection of specific actions (Mink 1996; Redgrave et al., 1999; Samejima and Doya, 2007), timing of action initiation (Ivry and Spencer 2004, Meck et al. 2008) and the evaluation of results (Lau and Glimcher 2007; Rangel et al. 2008). However, despite much experimental and theoretical progress (Leblois et al., 2006; Lo and Wang, 2006), the precise mechanisms by which BG circuits influence behavior remain unclear.

Correspondence should be addressed to JB (jdberke@umich.edu).

Author Contributions

The study was designed by JB and GG, and supervised by JB. Electrophysiological experiments were performed by GG, and drug infusion experiments by CS. GG and AW conducted the data analyses, and the manuscript was written by JB.

Unusually for forebrain structures, projection neurons in most BG nuclei use GABA for fast neurotransmission rather than glutamate (reviewed in Wilson, 2004). Within the striatum (the largest BG structure) the great majority of neurons are GABAergic medium-spiny neurons (MSNs) that integrate many convergent cortical and thalamic inputs, provide the striatal output to other BG nuclei, and also make axon collaterals onto other striatal MSNs. The resulting GABAergic network has been proposed to help achieve the selective facilitation of intended actions via mutual "winner-take-all" inhibitory interactions (for critical discussion of this idea, see Wickens et al., 2007; Wilson, 2007). Certainly, local striatal $GABA_A$ blockade within sensorimotor striatum seems to release abnormal movements, such as chorea and tic-like jerks (e.g. Worbe et al. 2009; McCairn et al. 2009). However, MSN-MSN interactions are typically sparse and unidirectional, with a relatively weak influence over spiking (Jaeger et al., 1994; Tunstall et al. 2002; Koós et al., 2004), and it now appears that the dominant component of GABAergic control over striatal output arises from relatively rare interneurons instead. In particular, parvalbumin-containing fast-spiking interneurons (FSIs) comprise only about 1% of striatal neurons (Luk and Sadikot 2001), but receive cortical inputs and in turn provide strong perisomatic GABAergic synapses onto hundreds of surrounding MSNs (Bennett and Bolam, 1994; Koós and Tepper, 1999; Gittis et al. 2010; Planert et al. 2010). This FSI-mediated feed-forward inhibition has been argued to make important contributions to action selection and execution via the broadly tuned, distributed suppression of MSNs representing unwanted actions (Kita et al., 1990; Parthasarathy and Graybiel, 1997). Consistent with such a role, a reduced number of striatal FSIs has been found in a rodent model of paroxysmal dystonia (co-contractions of opposing muscle groups; Gernert et al., 2000) and in postmortem tissue from human Tourette Syndrome patients (who have difficulty suppressing tics; Kalanithi et al., 2005; Kataoka et al. 2010).

Relatively little is known about the activity of striatal FSIs in awake behaving animals (Berke et al., 2004; Schmitzer-Torbert and Redish, 2008). Compared to MSNs, presumed FSIs have a far more consistent response to stimulant and antipsychotic drugs, with firing rate changes that positively correlate with (respectively) increased or depressed locomotor activity (Wiltschko et al. 2010). Nonetheless, during maze task performance FSIs have highly individualized patterns of responding, without appearing to act as a coordinated population (Berke, 2008). Since maze tasks have substantial drawbacks when investigating the fine temporal evolution of neural activity, here we examine patterns of FSI activity in rats performing a simple operant choice task in which the timing of key events was closely monitored. To gain greater insight into these patterns we compare them to other, simultaneously recorded elements of cortical-BG circuits: striatal MSNs and neurons in primary motor cortex (M1) and globus pallidus (GP).

RESULTS

Sensorimotor striatum and contraversive responses

To study striatal FSI contributions to choice behavior, we designed a simple conditional discrimination task (Fig. 1) that we expected to require intact function of the lateral (sensorimotor) striatum. Lateral striatum is involved in the acquisition and expression of cue-guided responses (Adams et al., 2001;Berke et al., 2009;McDonald and White, 1993), particularly movements to contralateral space (Brasted et al., 1997;Brown and Robbins, 1989;Carli et al., 1989;Cook and Kesner, 1988;Packard and McGaugh, 1996), and this subregion also has the highest density of FSIs (*e.g.* Kita et al., 1990;Berke et al. 2004). Hungry rats were placed in an operant box with five nosepoke holes, and each trial began with the illumination of one of the three more-central holes. The rat placed and held its nose in that hole while a brief instruction tone played, then performed a rapid nosepoke to one of the immediately adjacent holes, either to the left or right depending on the instruction tone.

To verify that the striatum is important for the left-right choice in this task, in a group of well-trained rats (n=6) we performed unilateral striatal infusions of the agonist $GABA_A$ muscimol, or artificial cerebrospinal fluid (ACSF) as a control (Supplementary Fig. 1a). Infusion of ACSF did not affect task performance ($p=0.926$; all comparisons ANOVA with Tukey post hoc test). Infusion of muscimol caused a selective, reversible reduction in cued contraversive responding (responses towards the side opposite to the infusion, $p<0.001$) without interfering with ipsiversive performance ($p=0.990$). Hence the lateral striatum is preferentially involved in contraversive responding in this task, and receptor stimulation in this subregion can $GABA_A$ powerfully affect choice behavior.

To examine the activity of FSIs during the performance of this choice task, four additional well-trained rats were implanted with tetrodes into multiple target regions simultaneously (Fig. 2). Most tetrodes were aimed towards lateral portions of striatum (Supplementary Fig. 2a), though for comparison we also recorded neurons in other striatal subregions, GP, and "neck" regions of M1 (Sanes et al., 1990). To help distinguish between sensory and motor aspects of neural coding, the task variant used in the electrophysiological studies had a brief, variable delay between the instruction cue and a "go" cue for movement onset. A total of 437 distinct, well-isolated cells (striatum, 339; M1, 73; GP, 25) were obtained from 39 sessions (mean number of trials/session: 125.8; mean % correct: 74.4, range: 64.3–87.1, Fig. 1d).

Examination of striatal neuron waveforms revealed distinct clusters of cell properties that closely resembled those seen in our previous studies (in different rats; Berke et al., 2004; Berke, 2008). The largest class of striatal cells (n=257) had relatively long duration waveforms (Fig. 2g; Table 1) and typically also had phasic firing patterns (Fig. 2h); these were presumed to be MSNs, which comprise >90% of striatal neurons. The second most numerous group (n=38) had the very brief waveforms (Kawaguchi et al., 1995; Mallet et al., 2005) and graded intrastriatal distribution (Fig. 2h inset; Kita et al., 1990) characteristic of FSIs (for discussion see Berke et al., 2004). These cells had higher firing rates than MSNs (Table 1) and were usually tonically active, with few extended pauses (Fig. 2h). A final class of striatal cells also had high baseline firing rates, but a characteristic waveform shape with intermediate peak and valley widths; as before (Berke, 2008) we labeled these as "O" cells for other, currently unknown phenotype. Because they were few in number (n=7), O cells were excluded from most analyses (but see Supplementary Figure 5). Distinct clusters were also observed for waveforms from motor cortex cells (Fig. 2d). The briefer-waveform cortical cells are very likely to be GABAergic interneurons (Barthó et al., 2004; Cardin et al., 2009), though for our analysis M1 cells were treated as one group except where noted below. GP cells all had high firing rates and relatively narrow waveforms (Fig. 2e), consistent with prior observations (*e.g.* Turner and Anderson, 1997).

FSIs disproportionately increase firing around choice execution

We wished to determine whether FSIs are preferentially active at any particular moment during the performance of the choice task. To generate a temporal response profile for each neuron we calculated perievent time histograms (PETHs; see Fig. 3 for examples) around each task event, and normalized this event-related firing by the peak response across all PETHs. Figure 4a shows this profile for all task-responsive cells of each class, sorted by moment of peak response. Since there are variable delays between task events, the highest firing rate obtained across all PETHs allows us to determine which task event produces the strongest response for each neuron. This epoch of peak response is shown for each cell in Fig. 4b.

Each studied brain area contained many cells with task-related changes in firing rate, especially near arrivals at the baited food port. We did not attempt to distinguish between

motoric and hedonic aspects of reward retrieval and consumption, but simply refer to all cells with maximal firing around reward receipt as “reward-related”. However, in marked contrast to the MSN population, FSIs were disproportionately active around the earlier time at which the rats initiated their left/right choice (“choice execution”; event 5). For units active during task performance, 35.1% (13/37) of FSIs showed maximal firing when aligned to this event - a significantly higher proportion than the 4.1% (3/74) of MSNs ($Z=4.39$, $p=0.0002$, two-sample proportion test corrected for multiple comparisons). Since we were interested in both increases and decreases in firing rate, we repeated these analyses using an alternative form of PETH normalization, based on the absolute value of firing rate Z-scores; very similar results were obtained (Supplementary Fig. 3). It was striking that while rats perform a series of movements during each trial (including nose in, choice, side in, nose out), only choice execution was associated with a significantly higher proportion of FSIs active over MSNs (Fig. 4d). Thus, even though FSIs tend to be more active when rats are moving (Wiltschko et al. 2010), movement onset alone cannot account for the selective engagement of FSIs at choice execution.

We considered several additional reasons why FSIs might be more likely to show this “choice-related” firing than MSNs. Firstly, FSIs and MSNs have very different average firing rates - could this be affecting our analyses? We think not, since both GP cells and presumed cortical interneurons had similar high firing rates to FSIs, yet neither group showed a comparable preference for the choice event (Fig. 4; Supplementary Fig. 5). Secondly, FSIs tend to be found more often in lateral striatum. We therefore examined whether the preferential activity of FSIs with choice execution was a reflection of the distinct information processing occurring in that brain subregion. While the small number of choice-related MSNs were all found in dorsal-lateral striatum, choice-related FSIs were much more broadly distributed (Supplementary Fig. 7). This indicates that the different balance of choice-related and reward-related firing for FSIs and MSNs is not caused by the increased FSI density in lateral striatum, and suggests that a choice-related increase in striatal FSI activity may act as a relatively global signal. Finally, averaging across the whole session may diminish some strong MSN responses that occur only on certain trial types. To assess this possibility we repeated our analysis, this time assigning cells to events on the basis of the strongest PETH response during either low tone trials, high tone trials, leftward trials or rightward trials. Although this did change the assignment of some specific neurons to events, FSIs still disproportionately preferred the choice execution event (Supplementary Fig. 4).

Choice-related activity might reflect the participation of FSIs in the selective initiation of a chosen action, or a later process such as monitoring of choices (e.g. using efference copy via side-branches from the corticospinal tract – Reiner et al. 2003). To help distinguish between these possibilities we examined the fine timing of firing rate increases in each cell population. Although most choice-related FSIs reached their *peak* firing rate slightly after choice execution (Fig. 4b), a change-point analysis indicated that the abrupt increases in their activity began substantially earlier (Fig. 3e). Both of the FSI and M1 populations showed a clear cluster of change times shortly before choice onset (median values −117ms, −55ms respectively relative to movement detection), and the distribution of FSI change times was significantly earlier than the M1 distribution ($p = 0.0366$, 1-sided Komogorov-Smirnov test).

Assigning neurons to a single event actually underestimates the proportion of FSIs that increase firing near choice execution, since many such FSIs showed even greater activity at another point in the trial (Supplementary Fig. 8). When we examined the overall response of each neuronal population a clear “pulse” of enhanced FSI activity was observed around choice execution, while peak MSN population activity was found around reward retrieval

(Fig. 4c). This population level analysis further revealed a striking pattern of opposite changes in the FSI and GP populations. GP cells tended to have elevated firing rates during the hold period after instruction tone onset; as the rats finally initiated an action, GP population activity fell sharply as FSI activity increased. This result is especially intriguing as there is a specific direct GABAergic projection from GP to striatal FSIs (Bevan et al., 1998), suggesting that disinhibition in this feedback pathway may contribute to the FSI pulse.

FSIs are selective for movement direction

A coordinated pulse of striatal FSI activity is consistent with theories that view these cells as providing broadly-tuned, blanket suppression of MSNs (e.g. Parthasarathy and Graybiel, 1997; Wickens and Arbuthnott, 1993). However, individual FSIs clearly have diverse patterns of firing rate change, both in the present data (Supplementary Fig. 8) and in our prior results (Berke, 2008). To explore information processing by individual FSIs, we examined selectivity for one chosen action over the other. The great majority of FSIs had high movement selectivity, and both contraversive and ipsiversive-preferring neurons were observed in similar numbers (Fig. 5). To tease apart other factors that may contribute to the firing rate of FSIs and other subpopulations during action selection, we performed multiple regression analysis using a range of variables including the instruction tone, movement direction, the spatial position from which the choice was executed, reaction time, movement time, and trial outcome (Supplementary Fig. 6). For each of the MSN, FSI, M1 and GP populations, movement direction was the most common dominant factor, with very few cells more concerned with other task aspects such as the specific tone or the rat's spatial position (e.g. Fig. 5d). In particular, among FSIs that had significant factors in the multiple regression, 11/14 (78.6 %) were most concerned with the specific movement direction These results indicate that, rather than FSIs acting continuously as a single global signal, the transient coordination of FSI activity is superimposed on a background of idiosyncratic individual firing rate time courses (Berke, 2008) that are highly influenced by movement direction.

Since we found direction-selective neurons in all examined brain areas, we next asked whether neural populations in one area become selective before another (Fig. 5b; Supplementary Fig. 6). In each area, individual neurons tended to become direction-selective in close temporal proximity to choice movement onset and reach peak selectivity shortly after movement onset. We found no compelling evidence that direction selectivity developed more quickly in one population than another. Although our limited data set may have obscured small timing differences, this result provides additional evidence that information about the selected action tends to co-evolve within cortical-basal ganglia feedback loops (e.g. Leblois et al., 2006) rather than appearing in a serial chain.

FSIs show opposite direction-selectivity to nearby MSNs, but do not provide constant fast inhibition

The muscimol injection experiment indicates that the lateral striatum is particularly important for contraversive movements in our task. Yet, both contraversive- and ipsiversive-preferring neurons were found intermingled in lateral striatum (and other striatal subregions) in similar numbers, and there was no gross relationship between recording location within striatum and direction preference ($p > 0.05$ for both MSNs and FSIs, regression t-tests for directional selectivity vs. each [AP,ML,DV] dimension of recording location). On a finer scale, MSNs and FSIs are each components of local microcircuits (Gustafson et al., 2006) that may serve as functional modules (Wilson, 2000; Albin & Mink 2006). We considered several ways in which these microcircuits might be organized. If nearby FSIs and MSNs receive similar inputs from cortex, with (for example) feed-forward inhibition regulating

MSN activity to enhance dynamic range (Pouille et al. 2009; Gittis et al. 2010) then one might expect FSIs and MSNs to tend to fire together and have similar selectivity. Alternatively, if FSIs are important for the active suppression of unwanted MSN action representations, they might be expected to have opposite direction preferences (e.g. Diester and Nieder, 2008). We examined all pairs of cells for which both neurons had significant direction selectivity, and were recorded simultaneously from the same tetrode (since for these pairs the MSN was likely to be in range of the FSI axonal field; Berke, 2008, Gittis et al. 2010). Consistent with a role in the active suppression of alternatives, FSI-MSN pairs always had opposite direction preferences (Fig. 6; 8/8 pairs opposite; p=0.0039, 50% binomial distribution). This was not the case for MSN-MSN pairs, which tended to have the same direction preference (4/15 pairs opposite).

We next looked for more direct evidence of inhibitory interactions using crosscorrelograms. A suppression in target cell firing for 2–3 ms after a reference cell spike has been previously used to identify likely monosynaptic $GABA_A$-mediated inhibition in neocortex (e.g. Barthó et al., 2004), and we were readily able to observe examples of this for presumed interneuron : projection cell pairs in our own M1 data (Fig. 7a). However, of 86 striatal FSI:MSN pairs recorded on the same tetrode, none showed convincing evidence of monosynaptic FSI to MSN inhibition in session-wide crosscorrelograms (Fig. 7b). Since for many of these pairs we had limited power to detect inhibition due to low firing rates of MSNs, we combined crosscorrelograms across all pairs, reasoning that if similar, strong interactions exist in a substantial fraction of pairs, this should be visible after averaging. When we did this for presumed interneuron: projection cell pairs in cortex the expected fast inhibition was readily apparent (Fig. 7c), but we found no comparable evidence for inhibition in striatum (Fig. 7d). This result stands in contrast with prior *in vitro* studies of striatum showing robust fast inhibition between FSIs and a large proportion of surrounding MSNs (Koós and Tepper, 1999; Gittis et al. 2010; Planert et al. 2010). We therefore repeated our analysis using data from another set of striatal recordings in awake behaving rats (described in Wiltschko et al. 2010). None of the 133 same-tetrode FSI:MSN pairs in the second data set showed clear inhibition either, and once again averaged crosscorrelograms did not reveal fast inhibition (Supplementary Fig. 7). We conclude that, if strong and fast FSI-mediated inhibition is operating in the striatum of behaving animals, it is not as continuously present as superficially-similar mechanisms in cortex.

DISCUSSION

Information processing within cortical-basal ganglia circuits makes use of multiple internal control signals, including the neuromodulators dopamine and acetylcholine. Here we have found another potential internal control signal: a pulse of enhanced activity of presumed striatal FSIs, that is broadly distributed within striatum and is correlated with reduced GP activity. Importantly, this FSI pulse was not seen in conjunction with every performed action, but specifically occurred just before choice execution – a moment at which one highly-trained action must be enabled and another suppressed. Additional studies are required to define the exact circumstances that cause a coordinated modulation of FSI activity. However, our results are intriguing given observations of an FSI deficit in Tourette Syndrome (Kalanithi et al., 2005; Kataoka et al. 2010), as this disorder is characterized by difficulties in the suppression of learned motor patterns, and is hypothesized to reflect the overactivity of focal groups of striatal MSNs (Albin and Mink 2006).

Heterogeneous versus coordinated changes in FSI firing rates may reflect different type of input

Despite the transient coordination of FSI rate increases, most FSI firing rate changes during operant task performance were not shared between different FSIs - even neighboring cells.

This is consistent with our prior work, in which we found highly idiosyncratic FSI activity in a radial maze task (Berke, 2008). Both tasks demonstrate that the patterns of FSI firing are far more complex than had earlier been expected, given their interconnection by gap junctions and *in vitro* inhibition of many nearby MSNs (Koós and Tepper, 1999; Plenz 2003; Gittis et al. 2010; Planert et al. 2010). However, in the radial maze we found no clear evidence for any moment of coordinated FSI firing rate change, despite related task demands such as cue-guided responses. The most important difference may be that the operant task used here was specifically designed to obtain greater temporal definition of behavioral events, including the moment of choice execution. Unlike the maze task, the operant task also includes an enforced hold period that helps to define just when the chosen action is initiated, and this delay may have introduced additional demands for behavioral inhibition involving FSIs.

What accounts for these two aspects of striatal FSI firing - idiosyncratic individual activity time courses, but transiently coordinated firing rate increases at choice execution? We propose that this reflects two different types of input to FSIs. On the one hand, FSIs are receiving complex combinations of sensory and motor information from multiple cortical regions (Ramanathan et al., 2002). On the other hand, FSIs selectively receive a continuous barrage of GABAergic inputs from high-firing-rate GP neurons (Bevan et al., 1998). The pallidostriatal pathway is more divergent than the striatopallidal pathway (Spooren et al., 1996), allowing GP neurons to coordinate neural activity over more widely distributed regions of striatum (Rajakumar et al. 1994). GP cells themselves receive inputs from subthalamic nucleus, which can provide a broad brake over behavior (Aron and Poldrack, 2006), and increases in GP activity have been previously noted under hold conditions, in which a specific movement is programmed but not yet executed (*e.g.* Turner and Anderson, 2005). It is therefore plausible that the sharp reduction in population GP firing at the end of the hold period is responsible for the FSI pulse, via disinhibition. Although future studies should directly manipulate the GP to confirm its contributions, a role for the pallidostriatal pathway in the coordinated control of striatal FSIs is also consistent with investigations of BG activity following dopaminergic manipulations. In particular, systemic injection of the antipsychotic eticlopride (a D2 antagonist) causes an increase in GP activity (Billings and Marshall 2003) together with a highly uniform suppression of FSI firing rate (Wiltschko et al. 2010). While BG theorists have begun to consider how FSI modulation by GP may contribute to action initiation (Shouno et al. 2009; Wilson 2009) the present findings indicate that the pallidostriatal pathway merits greater attention.

FSI contributions to striatal microcircuits

The behavioral impact of altered striatal FSI activity presumably arises from their influence over MSNs. *In vitro* FSIs are typically quiet, due to the loss of their afferent inputs, but evoking spikes by somatic current injection strongly inhibits or delays evoked spiking in connected MSNs (Koós and Tepper, 1999). In anesthetized rats there is evidence for potent FSI-mediated feedforward inhibition of MSN following cortical stimulation (Mallet et al. 2005), and an examination of MSN membrane voltage during UP states suggests that the fine timing of MSN spiking is largely determined by inhibitory inputs, that are likely FSI synapses (Wilson 2009). Despite these prior results, in awake behaving animals we found no evidence for strong short-latency FSI inhibition of MSNs using crosscorrelograms. In part, this may reflect limitations of our analytical tools or datasets, such as relatively few spikes for many FSI-MSN pairs and the fact that not all nearby pairs are synaptically connected. However we think these are unlikely to be the sole explanations, given that we were readily able to detect likely fast inhibition in cortex despite much smaller amounts of available cortical data. An alternative possibility is that the absence of obvious FSI-MSN inhibition reflects the strongly depressing nature of these synapses (Plenz and Kitai 1998; Koos and

Wilson 2004; Gittis et al. 2010; Planert et al. 2010). FSIs are generally continuously active in awake rats, allowing little time for synaptic recovery between spikes. In fact, when natural FSI spike trains from awake rats are used in simulations of FSI-MSN synaptic transmission, the resulting post-synaptic potentials are in a highly depressed state for significant amounts of time (A. Klaus, G. Silberberg, J. Hellgren-Kotaleski, personal communication). The strong FSI-MSN inhibition seen in slices and in anesthetized animals may therefore reflect in part the unusually low FSI firing rates under those conditions (e.g. compare our average FSI rate of 18.3 Hz to the 0.474 Hz observed during urethane anesthesia-induced slow waves; Mallet et al. 2005). Whether or not synaptic depression is responsible, our results indicate that during normal behavior most FSI spikes do not produce a rapid, synchronous “veto” of spiking in the cloud of surrounding MSNs. Our observation that FSIs always had opposite direction preferences to nearby MSNs suggests that they are nonetheless active participants in information processing within striatal microcircuits (Humphries et al. 2009). It is also important to note that we examined session-wide crosscorrelograms. It has been shown that monosynaptic interactions can be modulated by ongoing behavior, and the accompanying specific patterns of presynaptic activity that produce short-term facilitation or depression (Fujisawa et al. 2008). While additional data will be required to adequately assess whether strong FSI-MSN inhibition is indeed present in behaving animals at specific moments, the emerging findings on striatal synaptic dynamics provide further evidence for the likely importance of precise FSI firing patterns (Berke 2009; Lau et al. 2010).

Striatal circuitry and the organization of action

Our operant choice task was designed to be simple, yet it still involves multiple component processes. Voluntary action involves a series of decisions, such as whether to act, what to do and when to do it (Haggard 2008). There is some evidence that distinct cortical-basal ganglia loops are differentially involved in these stages of action, with sensorimotor striatum preferentially involved in the execution of actions, rather than their selection or preparation (e.g. Gerardin et al. 2004). This is compatible with our observations – even though FSIs across striatum showed preferentially enhanced firing during choice execution, FSIs are more densely present in sensorimotor striatum suggesting that they are especially important for the functioning of this subregion. We note that choice execution is the moment at which the sequence of actions performed within a trial bifurcates along two highly learned paths. The extended training and reinforcement establishes striatum-dependent learned movement sequences (Graybiel 1998) that are prepotent within the task context, yet one of these must be suppressed on each trial. We suggest that FSI-mediated suppression of unwanted alternative representations may be particularly critical in sensorimotor striatum because choice execution involves a “point of no return” (Osman et al. 1986) – and once we actually start to act, it is particularly important not to vacillate between alternatives. In this way FSIs may contribute to an overall BG function as a gate between a repertoire of potential motor programs and overt actions (*e.g.* Hikosaka 1998; Ivry and Spencer 2004).

Although our working hypothesis is that a broadly distributed FSI pulse helps to suppress prepotent but currently inappropriate actions, other possibilities should be explored in future work. These include a network reset, that facilitates the transition between ensembles representing distinct components of an action sequence (Carrillo-Reid et al., 2008; Wickens and Arbuthnott, 1993), and a role in guiding striatal plasticity, as broad signals about overall population response can assist reinforcement-based learning (Urbanczik and Senn, 2009). Nonetheless, our results suggest a circuit arrangement in which specific complex patterns of information feed-forward through largely parallel, segregated striatal-pallidal channels, while less information-specific, divergent control signals flow in the opposite direction.

EXPERIMENTAL PROCEDURES

Behavioral task and drug infusions

Animals were housed on a 12 hr:12 hr light/dark cycle, with experiments performed during the light phase. For daily training sessions, adult male Long-Evans rats (~350 g) were placed in a recording chamber (MED-NPW-5L; Med Associates Inc., St Albans, VT, USA; modified to accommodate large rat implants) with stainless steel grid floors, five nosepokes, a pellet dispenser, a speaker, and a video camera (Fig. 1a). Infrared photobeams detected the presence of the rat's nose at each nosepoke hole and the food port. Rats were initially trained to nosepoke an illuminated hole to receive a 45 mg sucrose pellet delivered to a receptacle in the rear of the chamber. Rats were then trained to hold in the nosepoke and wait for a brief burst of white noise to get a reward. The time delay to the white noise was gradually increased until the rats waited for 900–1250 ms for >85% of the trials. In the next phase of training (see Fig. 1b,c), rats waited for the white noise cue as before; however, now either a high (4 kHz) or a low (1 kHz) 250 ms tone was played during the hold period. The time between nose in and tone onset (pre-tone delay) varied between 250–350 ms. The white noise burst instructed the animals that they were free to choose one of the adjacent nosepokes. For the 1 kHz tone, trials were rewarded for leftward movements, while 4 kHz tones rewarded rightward movements. The total hold time required to correctly complete the trial was pseudo-randomly selected to be between 900–1250 ms (uniform distribution). If the rats failed to hold until the white noise burst, trials were aborted and a 10–15 s timeout began (with houselight on). To discourage the development of a side preference, rats were cued to move in a given direction only if at least one of the three previous responses was to the opposite side. Inter-trial intervals were selected pseudo-randomly from the range 15–30 s. Roughly 10% of the session consisted of free-choice "catch" trials, in which both tones were played simultaneously and left and right choices were each rewarded at p=0.5. Catch trials were not analyzed here. After each training session rats were fed 14 g of standard chow, which kept them at approximately 90% of free feeding weight.

For drug infusions, six rats were trained to perform the behavioral task above, with the exception that the 1 kHz or 4 kHz tone indicated the end of the hold period (i.e. no separate "Go" cue). Once performance had asymptotically stabilized, a guide cannula was implanted unilaterally into the striatum (target coordinates AP +0.5, ML +3.5, DV 4.5 mm, including the additional 1 mm ventral protrusion of the infusion cannula) on either the left (n=3) or right side (n=3). After two weeks recovery rats resumed a series of behavioral testing sessions which included (on different days, in order) a mock injection (in which the cannula was connected to the infusion apparatus but without infusion); an injection of ACSF (0.5 μl over 5 min; ion concentrations in mM: Na 150; K 3.0; Ca 1.4; Mg 0.8; P 1.0; Cl 155); a muscimol injection (0.05 μg/0.5 μl over 5 min, starting 15 min before task onset); and another ACSF injection.

Electrophysiological data were obtained from four rats, each implanted with 21 individually drivable tetrodes (four 12.5 μm Ni-Cr wires twisted together; Wilson and McNaughton, 1993). All tetrodes were placed in the right hemisphere, directed toward the dorsal lateral striatum, the nucleus accumbens, the globus pallidus, and primary motor cortex (M1, target region: +3.0mm AP, 3.0mm ML). Three skull screws were placed in contact with frontal, parietal, and motor cortical regions to record ECoG signals. Additional skull screws served as ground (posterior lateral skull ridge) and reference (on the midline, approximately 1 mm posterior to lambda). Data acquisition was performed using a 96 channel system built around custom amplifiers and LABVIEW™ software (National Instruments, Inc.). This system also acquired synchronized digital video images (640×480 pixels, 15 frames/s). Neural signals were recorded in wide-band (1 to 9,000 Hz) to reduce distortions of waveform shape (Wiltschko et al., 2008) and digitized continuously at 31,250 Hz. In order

to ensure that all event times within the behavioral task were measured with the same high precision, the status of all the relays that controlled cues and monitored photobeams was also sampled at the same frequency (32 μs resolution).

Following implantation and one week of recovery, recordings were made for several weeks to several months during performance of the delayed choice task. At the end of the experiment, each tetrode site was marked with a small lesion by passing 25 μA of current for 10 s. Following perfusion and Nissl staining, final tetrode locations were mapped onto coordinates in a reference brain atlas (Paxinos and Watson, 2005) using Sqirlz Morph software (Xiberpix, Inc.), and the location of prior recording days were estimated from screw turns. Cells that were not unequivocally in the motor cortex, striatum, or globus pallidus were not included in analyses. To avoid introducing biases into the activity of neuronal subpopulations, we wished not to repeat analysis of the same cells. Thus, neurons were only included from one session for each tetrode, unless the tetrode had been moved by a minimum of 100 μm between sessions.

Spike Sorting and Classification

Spike-sorting was performed manually using Offline Sorter (Plexon Inc, Dallas TX), following digital high-pass (512 Hz) filtering of the continuous data. Differences in the waveform size and shape across the four tetrode wires were used for separating single units. The reliability of spike cluster separation was quantitatively determined by the refractory period in the auto-correlograms (Harris et al., 2000). Across all cells in our database, the mean proportion of inter-spike-intervals <1 ms was 0.00073 (range: 0 to 0.0053), suggesting well-separated neurons. Once spike times were obtained for each single unit, the mean wide-band waveforms were obtained simply as a spike-triggered average of the wide-band continuous signals. Striatal cells were further classified as either a putative medium spiny cell (MSN), fast-spiking interneuron (FSI), or an “other” presumed interneuron (O) based on three distinct clusters found in a scatter plot of two measurements of the wide-band spike waveform: (1) the peak width at one-half maximum (FSI: 50–200 ms; MSN: 150–450 ms; O: 200–300 ms), and (2) the time from peak to valley (FSI: 100–455 ms; MSN: 560–1500 ms; O: 300–550 ms). All cells are shown with negative voltage upward. Cells that were inverted (n=20) or did not show a clear valley (n=14) were not classified.

Data Analysis

All analyses were performed using MATLAB (Mathworks, Inc.; Natick, MA) or SPSS (SPSS, Inc.; Chicago, IL). To measure the proportion of time spent in long inter-spike intervals (ISIs), $Prop_{ISI>Xs}$ (Schmitzer-Torbert and Redish, 2008), for each spike train we found all ISIs which exceeded a criterion (here X=2 s), summed those ISIs, and divided by the total session time. We characterized each neuron’s responsiveness to task events by constructing peri-event time histograms (PETHs) around each of the eight events shown in Fig. 1. For each PETH we analyzed a 3 s window, with a bin size of 30 ms followed by smoothing by a 3-point moving average. To restrict the analysis to cells active during the task, we adopted an inclusion criterion that the peak of at least one PETH must be greater than 5 Hz (this roughly corresponds to a minimum of 1 spike in a given 30ms bin every seven trials, or more spikes on fewer trials). For each neuron, the maximum value for all bins across all eight PETHs was used for normalization. For Z-score-based analyses, PETHs were normalized by subtracting the session-wide mean firing rate from each time bin, dividing by the session-wide standard deviation, and taking the absolute value. For contraversive and ipsiversive PETHs (Fig. 5), a 2 s window was used centered on the choice execution event, and the results were rank-ordered by time of peak firing rate (within contralateral, then ipsilateral trials). The selectivity index (SI) was derived from these contraversive and ipsiversive PETHs (Fig. 5c). The SI of the nth bin was calculated by:

$$SI_n = \frac{Ipsi_n - Contra_n}{Ipsi_n + Contra_n},$$

and we report the overall SI as the maximum SI_n across all 30 ms bins.

Statistical Analysis

For the local drug infusion data, we used a mixed-model ANOVA with a subject factor (RAT), and repeated measures factors of CUE (ipsi vs. contra), ACTION (ipsi, contra, error), and SESSION (MOCK, ACSF1, MUSC, ACSF2). The OUTCOME (proportion of trials selecting the action) was our dependent variable. The analysis indicated significant main effects of ACTION (F=352.1, df=2, P<0.001) but not of SESSION or CUE (F=0.0, P=1 for both). The results showed a significant SESSION × ACTION interaction (F=17.7, df=6, P<0.001), a significant CUE × ACTION interaction (F=531.1, df=2, P<0.001), and a significant three-way interaction of SESSION × CUE × ACTION (F=10.107, df=6, P<0.001).

To compare the proportion of event-related cells between neuronal subtypes, we used a two-sample test of proportions (Crewson, 2006) in which the standard error (S_{p1-p2}) is

$$S_{p_1-p_2} = \sqrt{\widehat{pq}}\sqrt{\frac{n_1+n_2}{n_1 n_2}}, \widehat{p} = \frac{c_1+c_2}{n_1+n_2}, \widehat{q} = 1-\widehat{p},$$

where $c_1$and c_2 are the number of occurrences in the two groups, and n_1 and n_2 are the total number in each group. We then computed the test statistic of the proportion difference,

$$Z = \frac{(c_1/n_1 - c_2/n_2)}{S_{p_1-p_2}}.$$

To correct for multiple comparisons, we simply multiplied the resulting p-value by 8 (the number of task events examined) and considered it significant if it remained below 0.05.

For the multiple regression analysis, we analyzed the residual component, ε(*i*), using the animal's direction of movement *d*(*i*), the location of the starting position of each trial *p*(*i*), the tone that played T(*i*), the trial outcome (correct/wrong) *o*(*i*), the reaction time *RT*(*i*), the movement time *MT*(*i*), and the trial number *n*(*i*). For each bin from time *t* to *t*+Δ*t*, the magnitude of firing rate, *F*(*i*), for the i^{th} trial were fitted by the following multiple regression model:

$$F(i) = \beta_0 + \beta_d d(i) + \sum_{n=1}^{N-1} \beta_{p_n} p_n(i) + \beta_t t(i) + \beta_o o(i) + \beta_{RT} RT(i) + \beta_{MT} MT(i) + \beta_n n(i) + \varepsilon(i).$$

The regression slopes β_0, β_d, β_{p1}, β_{p2}, β_T, β_o $\beta_{RT,}$ β_{MT} β_n (for *N*=3 positions) and their t-values were estimated by the REGSTATS function of the MATLAB Statistical Toolbox. Analysis was performed 380 times using a sliding time window of Δ*t*=100 ms that stepped in 5 ms intervals from *t*=−1 s before execution of choice movement to *t*=1 s after. For each neuron, the peak movement selectivity was defined as the maximum t-statistic for β_d across all timesteps (e.g. Fig. 3). Similarly, the peak position selectivity was defined as the maximum t-statistic of and β_{p1} and β_{p2} across all timesteps. These peak selectivities were

used for the comparison of neural coding of choice-direction versus spatial position (Fig. 5d). To be included, a neuron had to have a regressor that remained significant ($p<0.01$) after correcting for multiple comparisons. This correction involved dividing by the number of unique time bins tested (380 tests total, but the 100 ms bins overlap at 5 ms intervals thus reducing unique time bins by a factor of 20).

Confidence intervals for single-unit PETHs were derived using the null hypothesis that spike trains arise from Poisson point processes with constant mean rate (detailed in Abeles 1982). Confidence intervals for population PETHs were constructed using a resampling method, with 100 shuffled datasets. In order to obtain estimates that were not dominated by a few outlier cells, shuffling was performed within each cell's normalized PETH by randomizing the order of 30 ms bins. This preserved the peak event response of that cell while scrambling the time at which this peak contributed to the population PETH. A given bin within the population PETH was considered to be significant if the value from the real data was either higher or lower than at least 95 of the shuffled data sets.

To determine the onset times of choice-related firing rate increases, we used a modified version of the cumulative change point algorithm (Gallistel et al., 2004). We included each neuron that reached peak firing around choice execution, in PETHs that used either all correct trials or specific subsets based on tone pitch or chosen direction (as in Supplementary Fig. 4). The algorithm generates a cumulative sum of each PETH bin, in a window starting 1s before choice onset and ending at the time of peak firing rate (within 1s of choice onset). The graph point that deviates maximally from a linear increase in firing within this window is nominated as the change point time. In one case the detected change-point was at the very start of the PETH window (i.e. −1s), and so was excluded from further analysis. For this behavioral task we did not attempt to constrain and/or identify specific muscle groups involved in the chosen movement, and record EMG from those specific muscles. Therefore, the numbers obtained for the timing of neural activity changes relative to movement are useful primarily for the comparison of relative timing between structures, rather than for their precise absolute values.

For identification of putative monosynaptic connections between cells, we looked for short-latency / short-duration events in crosscorrelograms (Csicsvari et al., 1998), using a bin width of 1ms. As our spike sorting methods do not permit the separation of spikes that occur simultaneously on the same tetrode, we excluded from analysis the time bins from −1 ms before to 1 ms after the reference cell spike. Since we were interested here in the significance of short-latency interactions, crosscorrelograms were corrected by shifting the spike train of the second cell with a fixed (100 ms) time interval, and subtracting the shifted histograms from the originals. Peaks within 3 ms of the center bin were defined as significant excitatory interactions when at least one of the bins (1 ms width) exceeded the 99.9^{th} percentile of the mean. Short-latency troughs were considered to be due to inhibition when at least two neighboring bins were $<0.1^{th}$ percentile of the mean. To help visualize FSI-MSN interactions that might not be detectable in individual crosscorrelograms due to relatively few MSN spikes, we computed the mean crosscorrelogram across all pairs. We used a window 100 milliseconds wide, centered on FSI spikes as reference events. A significant effect was defined to be at least 2 consecutive bins in the correlogram crossing above the 99.9^{th} percentile of the mean of 100 jittered surrogate crosscorrelograms. This threshold was defined independently for each time bin. To generate the surrogate crosscorrelograms, the spike time offsets (distance of each MSN spike to the FSI reference spike) were replaced by random numbers drawn from a uniform distribution over the interval [−50, 50] milliseconds. This maintains the total number of spikes used to generate the correlograms and preserves session-wide spike distributions, but removes any short-latency interactions between cell pairs.

Supplementary Material

Refer to Web version on PubMed Central for supplementary material.

Acknowledgments

We thank members of the Berke laboratory for comments and assistance with experiments. This project was supported by grants to JB from the Tourette Syndrome Association, the Whitehall Foundation, and the National Institute on Drug Abuse (R01-DA14318), and by the University of Michigan. GG was also partly supported by NIH grant R21-HD049842.

References

Abeles M. Quantification, smoothing, and confidence limits for single-units' histograms. J Neurosci Methods. 1982; 5:317–325. [PubMed: 6285087]

Adams S, Kesner RP, Ragozzino ME. Role of the medial and lateral caudate-putamen in mediating an auditory conditional response association. Neurobiology of Learning and Memory. 2001; 76:106–116. [PubMed: 11525249]

Albin RL, Mink JW. Recent advances in Tourette syndrome research. Trends Neurosci. 2006; 29:175–182. [PubMed: 16430974]

Aron AR, Poldrack RA. Cortical and subcortical contributions to Stop signal response inhibition: role of the subthalamic nucleus. J Neurosci. 2006; 26:2424–2433. [PubMed: 16510720]

Barthó P, Hirase H, Monconduit L, Zugaro M, Harris KD, Buzsaki G. Characterization of neocortical principal cells and interneurons by network interactions and extracellular features. J Neurophysiol. 2004; 92:600–608. [PubMed: 15056678]

Bennett BD, Bolam JP. Synaptic input and output of parvalbumin-immunoreactive neurons in the neostriatum of the rat. Neuroscience. 1994; 62:707–719. [PubMed: 7870301]

Berke JD. Uncoordinated firing rate changes of striatal fast-spiking interneurons during behavioral task performance. J Neurosci. 2008; 28:10075–10080. [PubMed: 18829965]

Berke JD, Breck JT, Eichenbaum H. Striatal versus hippocampal representations during win-stay maze performance. J Neurophysiol. 2009; 101:1575–1587. [PubMed: 19144741]

Berke JD, Okatan M, Skurski J, Eichenbaum HB. Oscillatory entrainment of striatal neurons in freely moving rats. Neuron. 2004; 43:883–896. [PubMed: 15363398]

Bevan MD, Booth PA, Eaton SA, Bolam JP. Selective innervation of neostriatal interneurons by a subclass of neuron in the globus pallidus of the rat. J Neurosci. 1998; 18:9438–9452. [PubMed: 9801382]

Brasted PJ, Humby T, Dunnett SB, Robbins TW. Unilateral lesions of the dorsal striatum in rats disrupt responding in egocentric space. J Neurosci. 1997; 17:8919–8926. [PubMed: 9348358]

Brown VJ, Robbins TW. Elementary processes of response selection mediated by distinct regions of the striatum. J Neurosci. 1989; 9:3760–3765. [PubMed: 2585053]

Cardin J, Carlén M, Meletis K, Knoblich U, Zhang F, Deisseroth K, Tsai L, Moore C. Driving fast-spiking cells induces gamma rhythm and controls sensory responses. Nature. 2009; 459:663–7. [PubMed: 19396156]

Carli M, Jones GH, Robbins TW. Effects of unilateral dorsal and ventral striatal dopamine depletion on visual neglect in the rat: a neural and behavioural analysis. J Neurosci. 1989; 29:309–327.

Carrillo-Reid L, Tecuapetla F, Tapia D, Hernández-Cruz A, Galarraga E, Drucker-Colin R, Bargas J. Encoding network states by striatal cell assemblies. J Neurophysiol. 2008; 99:1435–1450. [PubMed: 18184883]

Cook D, Kesner RP. Caudate nucleus and memory for egocentric localization. Behav Neural Biol. 1988; 49:332–343. [PubMed: 3408445]

Crewson, P. Applied Statistics Handbook. AcaStat Software; 2006.

Csicsvari J, Hirase H, Czurko A, Buzsaki G. Reliability and state dependence of pyramidal cell-interneuron synapses in the hippocampus: an ensemble approach in the behaving rat. Neuron. 1998; 21:179–189. [PubMed: 9697862]

Diester I, Nieder A. Complementary contributions of prefrontal neuron classes in abstract numerical categorization. J Neurosci. 2008; 28:7737–7747. [PubMed: 18667606]

Fujisawa S, Amarasingham A, Harrison MT, Buzsaki G. Behavior-dependent short-term assembly dynamics in the medial prefrontal cortex. Nat Neurosci. 2008; 11:823–833. [PubMed: 18516033]

Gallistel CR, Fairhurst S, Balsam P. The learning curve: Implications of a quantitative analysis. Proc Natl Acad Sci U S A. 2004; 101:13124–13131. [PubMed: 15331782]

Gerardin E, Pochon JB, Poline JB, Tremblay L, Van de Moortele PF, Levy R, Dubois B, Le Bihan D, Lehericy S. Distinct striatal regions support movement selection, preparation and execution. Neuroreport. 2004; 15:2327–2331. [PubMed: 15640749]

Gernert M, Hamann M, Bennay M, Löscher W, Richter A. Deficit of striatal parvalbumin-reactive GABAergic interneurons and decreased basal ganglia output in a genetic rodent model of idiopathic paroxysmal dystonia. J Neurosci. 2000; 20:7052–7058. [PubMed: 10995851]

Gittis AH, Nelson AB, Thwin MT, Palop JJ, Kreitzer AC. Distinct roles of GABAergic interneurons in the regulation of striatal output pathways. J Neurosci. 2010; 30:2223–2234. [PubMed: 20147549]

Graybiel AM. The basal ganglia and chunking of action repertoires. Neurobiol Learn Mem. 1998; 70:119–136. [PubMed: 9753592]

Gustafson N, Gireesh-Dharmaraj E, Czubayko U, Blackwell KT, Plenz D. A comparative voltage and current-clamp analysis of feedback and feedforward synaptic transmission in the striatal microcircuit in vitro. J Neurophysiol. 2006; 95:737–752. [PubMed: 16236782]

Haggard P. Human volition: towards a neuroscience of will. Nat Rev Neurosci. 2008; 9:934–946. [PubMed: 19020512]

Harris KD, Henze D, Csicsvari J, Hirase H, Buzsaki G. Accuracy of tetrode spike separation as determined by simultaneous intracellular and extracellular measurements. J Neurophysiol. 2000; 84:401–414. [PubMed: 10899214]

Hikosaka O. Neural systems for control of voluntary action--a hypothesis. Adv Biophys. 1998; 35:81–102. [PubMed: 9949766]

Humphries MD, Wood R, Gurney K. Dopamine-modulated dynamic cell assemblies generated by the GABAergic striatal microcircuit. Neural Networks. 2009; 22:1174–88. [PubMed: 19646846]

Ivry RB, Spencer RM. The neural representation of time. Curr Opin Neurobiol. 2004; 14:225–232. [PubMed: 15082329]

Jaeger D, Kita H, Wilson CJ. Surround inhibition among projection neurons is weak or nonexistent in the rat neostriatum. J Neurophysiol. 1994; 72:2555–2558. [PubMed: 7884483]

Kalanithi PSA, Zheng W, Kataoka Y, DiFiglia M, Grantz H, Saper CB, Schwartz ML, Leckman JF, Vaccarino FM. Altered parvalbumin-positive neuron distribution in basal ganglia of individuals with Tourette syndrome. Proc Natl Acad Sci USA. 2005; 102:13307–13312. [PubMed: 16131542]

Kataoka Y, Kalanithi PS, Grantz H, Schwartz ML, Saper C, Leckman JF, Vaccarino FM. Decreased number of parvalbumin and cholinergic interneurons in the striatum of individuals with Tourette Syndrome. J Comp Neurol. 2010; 518:277–291. [PubMed: 19941350]

Kawaguchi Y, Wilson CJ, Augood SJ, Emson PC. Striatal interneurones: chemical, physiological and morphological characterization. Trends Neurosci. 1995; 18:527–535. [PubMed: 8638293]

Kita H, Kosaka T, Heizmann CW. Parvalbumin-immunoreactive neurons in the rat neostriatum: a light and electron microscopic study. Brain Res. 1990; 536:1–15. [PubMed: 2085740]

Koós T, Tepper JM. Inhibitory control of neostriatal projection neurons by GABAergic interneurons. Nat Neurosci. 1999; 2:467–472. [PubMed: 10321252]

Koós T, Tepper JM, Wilson CJ. Comparison of IPSCs evoked by spiny and fast-spiking neurons in the neostriatum. J Neurosci. 2004; 24:7916–7922. [PubMed: 15356204]

Leblois A, Boraud T, Meissner W, Bergman H, Hansel D. Competition between feedback loops underlies normal and pathological dynamics in the basal ganglia. J Neurosci. 2006; 26:3567–3583. [PubMed: 16571765]

Lau B, Glimcher PW. Action and outcome encoding in the primate caudate nucleus. J Neurosci. 2007; 27:14502–14514. [PubMed: 18160658]

Lau T, Gage GJ, Berke JD, Zochowski M. Local dynamics of gap-junction-coupled interneuron networks. Phys Biol. 2010; 7:16015. [PubMed: 20228446]

Lo CC, Wang XJ. Cortico-basal ganglia circuit mechanism for a decision threshold in reaction time tasks. Nat Neurosci. 2006; 9:956–963. [PubMed: 16767089]

Luk KC, Sadikot AF. GABA promotes survival but not proliferation of parvalbumin-immunoreactive interneurons in rodent neostriatum: an in vivo study with stereology. Neuroscience. 2001; 104:93–103. [PubMed: 11311534]

Mallet N, Le Moine C, Charpier S, Gonon F. Feedforward inhibition of projection neurons by fast-spiking GABA interneurons in the rat striatum in vivo. J Neurosci. 2005; 25:3857–3869. [PubMed: 15829638]

McCairn KW, Bronfeld M, Belelovsky K, Bar-Gad I. The neurophysiological correlates of motor tics following focal striatal disinhibition. Brain. 2009; 132:2125–2138. [PubMed: 19506070]

McDonald RJ, White NM. A triple dissociation of memory systems: hippocampus, amygdala, and dorsal striatum. Behav Neurosci. 1993; 107:3–22. [PubMed: 8447956]

Meck WH, Penney TB, Pouthas V. Cortico-striatal representation of time in animals and humans. Curr Opin Neurobiol. 2008; 18:145–152. [PubMed: 18708142]

Mink JW. The basal ganglia: focused selection and inhibition of competing motor programs. Prog Neurobiol. 1996; 50:381–425. [PubMed: 9004351]

Osman A, Kornblum S, Meyer DE. The point of no return in choice reaction time: controlled and ballistic stages of response preparation. J Exp Psychol Hum Percept Perform. 1986; 12:243–258. [PubMed: 2943853]

Packard MG, McGaugh JL. Inactivation of hippocampus or caudate nucleus with lidocaine differentially affects expression of place and response learning. Neurobiology of Learning and Memory. 1996; 65:65–72. [PubMed: 8673408]

Parthasarathy HB, Graybiel AM. Cortically driven immediate-early gene expression reflects modular influence of sensorimotor cortex on identified striatal neurons in the squirrel monkey. J Neurosci. 1997; 17:2477–2491. [PubMed: 9065508]

Paxinos, G.; Watson, C. The Rat Brain in Stereotaxic Coordinates. 5. Elsevier Academic Press; 2005.

Planert H, Szydlowski SN, Hjorth JJ, Grillner S, Silberberg G. Dynamics of synaptic transmission between fast-spiking interneurons and striatal projection neurons of the direct and indirect pathways. J Neurosci. 2010; 30:3499–3507. [PubMed: 20203210]

Plenz D. When inhibition goes incognito: feedback interaction between spiny projection neurons in striatal function. Trends Neurosci. 2003; 26:436–443. [PubMed: 12900175]

Plenz D, Kitai ST. Up and down states in striatal medium spiny neurons simultaneously recorded with spontaneous activity in fast-spiking interneurons studied in cortex-striatum-substantia nigra organotypic cultures. J Neurosci. 1998; 18:266–283. [PubMed: 9412506]

Rangel A, Camerer C, Montague PR. A framework for studying the neurobiology of value-based decision making. Nat Rev Neurosci. 2008; 9:545–556. [PubMed: 18545266]

Reiner A, Jiao Y, Del Mar N, Laverghetta AV, Lei WL. Differential morphology of pyramidal tract-type and intratelencephalically projecting-type corticostriatal neurons and their intrastriatal terminals in rats. J Comp Neurol. 2003; 457:420–440. [PubMed: 12561080]

Rajakumar N, Elisevich K, Flumerfelt BA. The pallidostriatal projection in the rat: a recurrent inhibitory loop? Brain Res. 1994; 651:332–336. [PubMed: 7922583]

Ramanathan S, Hanley JJ, Deniau JM, Bolam JP. Synaptic convergence of motor and somatosensory cortical afferents onto GABAergic interneurons in the rat striatum. J Neurosci. 2002; 22:8158–8169. [PubMed: 12223570]

Redgrave P, Prescott TJ, Gurney KN. The basal ganglia: a vertebrate solution to the selection problem? Neuroscience. 1999; 89:1009–1023. [PubMed: 10362291]

Samejima K, Doya K. Multiple representations of belief states and action values in corticobasal ganglia loops. Ann N Y Acad Sci. 2007; 1104:213–228. [PubMed: 17435124]

Schmitzer-Torbert N, Redish AD. Task-dependent encoding of space and events by striatal neurons is dependent on neural subtype. J Neurosci. 2008; 153:349–360.

Shouno, O.; Takeuchi, J.; Tsujino, H. A spiking neuron model of the basal ganglia circuitry than can generate behavioral variability. In: Groenewegen, HJ.; Voorn, P.; Berendse, HW.; Mulder, AB.; Cools, AR., editors. The Basal Ganglia. Vol. IX. Springer Science+Business Media; 2009.

Spooren WP, Lynd-Balta E, Mitchell S, Haber SN. Ventral pallidostriatal pathway in the monkey: evidence for modulation of basal ganglia circuits. J Comp Neurol. 1996; 370:295–312. [PubMed: 8799857]

Tunstall MJ, Oorschot DE, Kean A, Wickens JR. Inhibitory interactions between spiny projection neurons in the rat striatum. J Neurophysiol. 2002; 88:1263–1269. [PubMed: 12205147]

Turner RS, Anderson ME. Pallidal discharge related to the kinematics of reaching movements in two dimensions. J Neurophysiol. 1997; 77:1051–1074. [PubMed: 9084582]

Turner RS, Anderson ME. Context-dependent modulation of movement-related discharge in the primate globus pallidus. J Neurosci. 2005; 25:2965–2976. [PubMed: 15772356]

Urbanczik R, Senn W. Reinforcement learning in populations of spiking neurons. Nat Neurosci. 2009; 12:250–252. [PubMed: 19219040]

Wickens JR, Arbuthnott GW. The corticostriatal system on computer simulation: an intermediate mechanism for sequencing of actions. Prog Brain Res. 1993; 99:325–339. [PubMed: 8108554]

Wickens JR, Arbuthnott GW, Shindou T. Simulation of GABA function in the basal ganglia: computational models of GABAergic mechanisms in basal ganglia function. Prog Brain Res. 2007; 160:313–329. [PubMed: 17499122]

Wilson, CJ. Striatal Circuitry: Categorically Selective or Selectively Categorical?. In: Miller, R.; Wickens, JR., editors. Brain Dynamics and the Striatal Complex. Harwood Academic; 2000.

Wilson CJ. GABAergic inhibition in the neostriatum. Prog Brain Res. 2007; 160:91–110. [PubMed: 17499110]

Wilson, C. What controls the timing of striatal spiny cell action potentials?. In: Groenewegen, HJ.; Voorn, P.; Berendse, HW.; Mulder, AB.; Cools, AR., editors. The Basal Ganglia. Vol. IX. Springer Science+Business Media; 2009.

Wilson MA, McNaughton BL. Dynamics of the hippocampal ensemble code for space. Science. 1993; 261:1055–1058. [PubMed: 8351520]

Wiltschko AB, Gage GJ, Berke JD. Wavelet filtering before spike detection preserves waveform shape and enhances single-unit discrimination. J Neurosci Methods. 2008; 173:34–40. [PubMed: 18597853]

Wiltschko AB, Pettibone JR, Berke JD. Opposite effects of stimulant and antipsychotic drugs on striatal fast-spiking interneurons. Neuropsychopharmacology. 2010; 35:1261–70. [PubMed: 20090670]

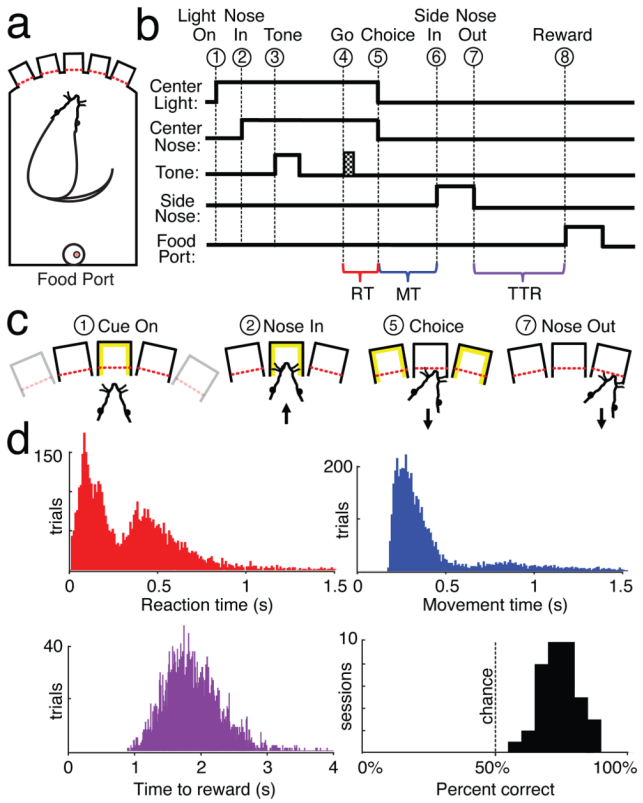

Figure 1. Behavioral task and performance

a) Depiction of operant chamber, with five nosepoke holes opposite food delivery port. b,c) Task event sequence, for correct performance. Each trial began with illumination of one of the three most central nosepoke holes (“Light On”, event 1). The rat had to place his nose in the illuminated hole (“Nose In”, event 2) and stay there (total hold duration = 900–1250 ms). During the hold window, a 250 ms instruction cue was played (“Tone”, event 3), followed after a variable delay (600–950 ms) by a Go cue (125 ms white noise burst; “Go”, event 4). The rat then pulled his nose out of the center hole (“Choice”, event 5) and poked an immediately adjacent hole (“Side In” event 6). If the direction of movement matched the instructional tone (learned arbitrary mapping: 1 kHz, go left, 4 kHz go right) then a sugar pellet was immediately delivered with an audible food hopper click, and could be collected by moving out of the side hole (“Nose Out”, event 7) and to the food port on the rear wall (“Reward”, event 8). Brackets indicate time epochs used to measure reaction time (RT), movement time (MT), and time to reward (TTR). d) Distribution of RT, MT, and TTR times (10 ms bins) and session performance (5% bins) from all animals. The mean time between events 6 and 7 was 337 ms (SD 311 ms). All four subjects had bimodal RT distributions, consistent with rats sometimes anticipating, and sometimes reacting to, the Go cue (Supplementary Fig. 1b).

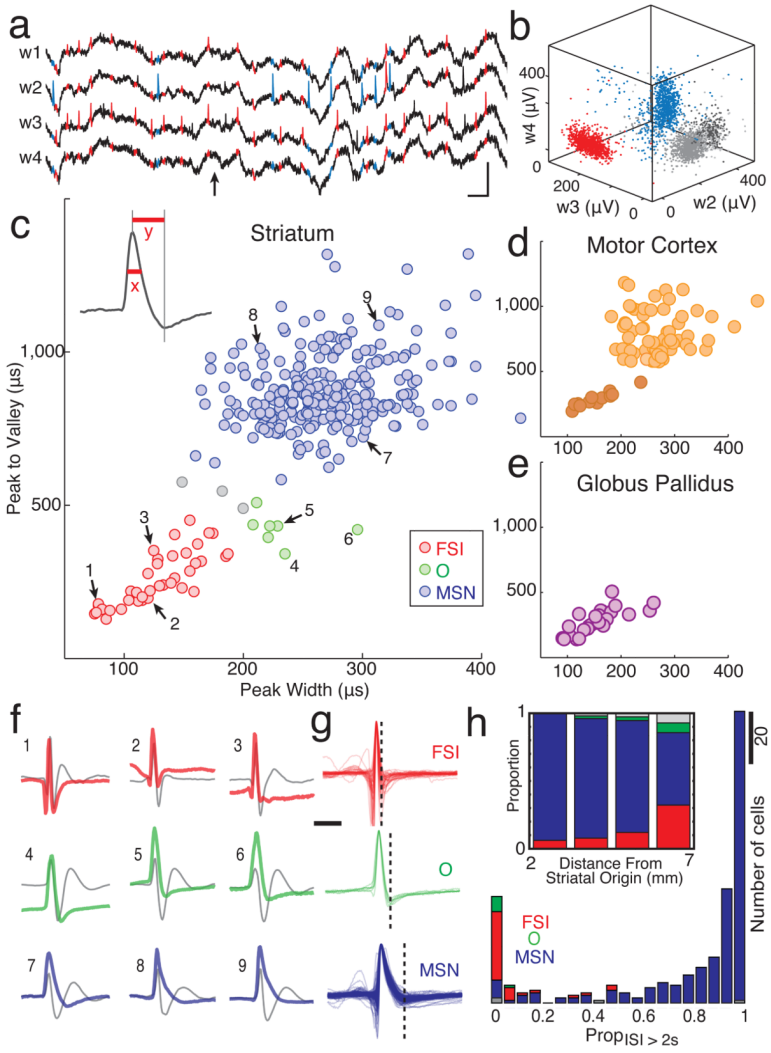

Figure 2. Classification of neurons

a) Example of wide-band recording (1–9,000 Hz) from a tetrode (four wires, w1–4) in striatum (arrow = arrival at food port; blue color highlights spikes from a presumed MSN, red highlights spikes from a presumed FSI). Scale bars: 0.5 mV, 10 ms. b) Single unit identification based on peak filtered spike voltage; three of the four tetrode wires shown. The red, blue clusters correspond to the spikes in a). c-e) Scatter plots of mean spike waveform durations (x, peak half-maximum; y, peak-to-valley time) for each single-unit. c) Striatal cells. Presumed MSNs are in blue, FSIs in red, O cells in green. d) M1 cells. Darker color indicates possible interneuron population. e) GP cells; all had brief spike durations. f) Mean wide-band spike waveforms for nine representative striatal cells. Numbers (1–9) correspond to cells indicated in c. For comparison to prior studies, digitally filtered versions of the waveforms are also shown (gray, 600–6,000 Hz Butterworth filter). g) All wide-band waveforms for the FSI, O, and MSN striatal cell classes, superimposed to show inter-cell variability. Vertical dashed bar = mean time of detected valleys. The complete database of neuron properties is available online as Supplementary Fig. 8). Phasic vs. tonic activity of striatal cell types. Histograms show, for each cell, the proportion of time spent in long interspike intervals (ISI > 2 s). Inset: Presumed FSIs were more common in sensorimotor (lateral/dorsal/caudal) striatum. Bars show proportion of each cell type by distance from an

origin point near the medial-ventral-rostral tip of the striatum (AP 3.13, ML 0, DV 8 mm below bregma; compare to Berke et al., 2004).

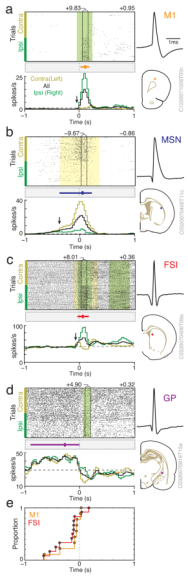

Figure 3. Analysis of peak firing rate and movement selectivity

a–d) Examples of choice-related cells. In each case mean wide-band spike waveform is at top right and recording location at bottom right. Center panels show spike rasters for all trials, aligned on choice execution (event 5) and separated by chosen direction (contraversive on top, ipsiversive on bottom). Epochs with a significant ($p < 0.01$) contra/ipsi firing rate difference are indicated by color shading (contraversive = gold, ipsiversive = green). Vertical black lines outline the 100 ms period with the most significant contra/ipsi difference (value of peak directional selectivity t-statistic is shown above the bin). The selectivity index value is shown above the rasters, on the right side. Bottom panels show corresponding peri-event time histograms (PETHs) for contraversive (gold), ipsiversive (green), and all trials (black). Bin size = 30 ms, with 3-point moving average smoothing. Session-wide mean firing rate is indicated by a dotted line. Arrows indicate times at which firing rates began to ramp up towards the peak rate, as detected by change-point analysis (see Methods). Above the histograms, the point of peak firing rate across all PETHs is shown with a vertical tick, and the period of greater than quarter-maximal response (i.e. > (mean rate * 0.75 + peak rate * 0.25) by a horizontal colored bar. Rasters and PETHs for all neurons are included in the database online (Supplementary Fig. 8). e) Comparison of change-point time distributions for the FSI and M1 cell populations. Included are FSI, M1 cells that reached peak firing rate in choice execution-aligned PETHs (few such cells were obtained for MSN, GP, so their distributions are not shown). Note the burst of detected FSI, M1 firing rate increases shortly before the onset of the chosen action.

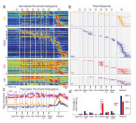

Figure 4. FSIs preferentially increase firing rate during choice execution

a) Peri-event time histograms (PETHs) for each cell, aligned on each of the eight events. For each cell, firing rate is shown by a color scale ranging from blue (zero) to red (peak rate), and within each class of cells neurons are rank ordered by time of peak firing. To be included, a cell had to have a firing rate of at least 5Hz in at least one PETH (using 30 ms bins). For display purposes, only a portion of each 3 s PETH window is shown (see Methods). For additional cell classes, see Supplementary Fig. 5. b) Events associated with peak firing rate. Order of cells is the same as (a). As in Fig. 3, vertical tick marks indicate the time bin with peak firing rate, and horizontal lines indicate the epoch for which firing rate was elevated by more than one-quarter of the difference between mean rate and peak rate (shown only for the PETH for which peak rate was reached). c) Mean normalized firing rate for each cell population in (a). Normalization before averaging helps to emphasize the population response, by minimizing the contribution of particular cells with especially strong responses. Bin size = 30 ms, smoothed with 3-point moving average. Shaded region = S.E.M., and bold lines indicate that population mean is outside 5% and 95% confidence intervals (see Methods). d) Proportions of MSN and FSI cells with peak firing for each event. The choice execution event was associated with a significantly different proportion of FSI and MSN peak firing (*** $p=0.0002$, two-sample proportion test, adjusted for multiple comparisons). All other events did not show a significant difference ($p>0.05$, adjusted for multiple comparisons). The inclusion criterion of at least 5Hz peak firing did not substantially change our results: with all neurons included, a significantly higher proportion of FSIs than MSNs still showed peak firing in association with the “choice” event ($Z=3.48$, $p=0.0009$, two-sample proportion test, corrected for multiple comparisons).

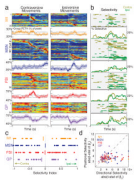

Figure 5. Directional selectivity around choice execution

a) Normalized PETHs for contraversive (leftward) and ipsiversive (rightward) movements for four cell classes. To be included, a cell had to have a peak firing rate of at least 5 Hz within 1 s of movement onset (toward either direction). For each cell class, the top plot shows normalized PETHs for individual neurons (rank ordered by the time of peak firing) and the bottom plots show population PETH. Grey lines indicate the 5th and 95th centile of confidence intervals; portions of the mean line that extend outside of this interval for at least two consecutive bins are indicated by increased thickness. Shaded area = S.E.M. b) Time epochs of significant directional selectivity. For each cell class, the top plots indicate epochs for which each neuron fired at a significantly higher rate on trials with contraversive (gold) or ipsiversive (green) movements ($p<0.01$, based on t-stat of regression b_d; see Methods); bottom plots indicate the instantaneous percentage of cells showing significantly higher firing rates for each movement direction (time bin = 5ms with 3-point smoothing). c) Selectivity index values for different cell classes. Vertical line indicates mean. d) Scatter plot of directional selectivity vs spatial (i.e. which of the three central holes) selectivity. Filled circles indicate that either the peak directional or spatial selectivity was significant ($p<0.01$).

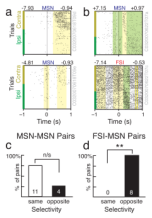

Figure 6. Nearby FSI-MSN cell pairs have opposite direction selectivity

a, b) Examples of two simultaneously recorded MSN cells (a) and a MSN and FSI cell pair (b). Raster format is the same as in Fig. 3. Note the inverse relationship between peak directional selectivity (above rasters, right) in the MSN/FSI pair. c, d) Selectivity directions for all 15 simultaneously recorded MSN-MSN pairs (c) and all 8 MSN-FSI pairs (d) for which both cells showed direction selectivity within 1s of choice execution. Double asterisks indicates significance, p=0.0039. n/s, not quite significant: p=0.0592.

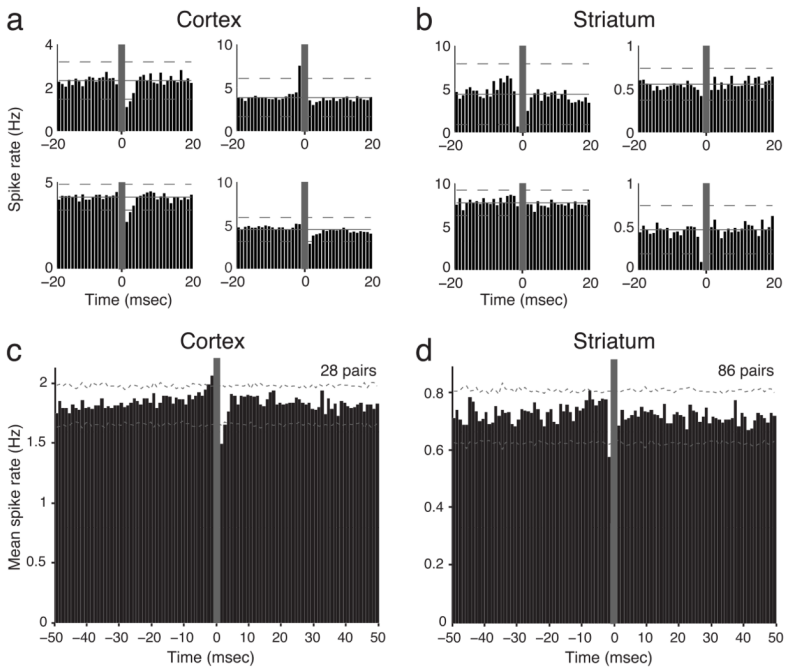

Figure 7. Fast inhibition from FSIs is clearly apparent in cortex, but not striatum

a, b) Examples of session-wide crosscorrelograms between individual pairs of presumed FSIs and projection neurons recorded on the same tetrode, in either cortex (a) or striatum (b). FSI spikes are at zero in all cases. Horizontal dashed lines indicate 99.9% confidence bounds. Grey-shaded areas indicate bins excluded from analysis due to potential spike overlap. c, d) Averaged crosscorrelograms for the two structures. Using both individual and averaged crosscorrelograms, we observed likely monosynaptic inhibitory and excitatory interactions in cortex but never in striatum.

Table 1
Firing rate and waveform properties of neuronal populations

Data are presented as mean (SD). Firing rate is the session-wide mean.

	n	Firing Rate / Hz	Peak Width / μs	Peak to Valley / μs
MI	72	2.7 (4.4)	250.3 (68.5)	695.7 (246.5)
MSN	257	1.1 (4.5)	270.7 (48.7)	873.2 (120.0)
FSI	38	18.3 (18.3)	128.1 (31.8)	259.9 (86.7)
O	7	22.1 (15.4)	231.8 (29.8)	423.8 (50.4)
GP	25	17.8 (13.4)	153.3 (47.8)	294.0 (96.6)